Acta Mech 229, 4071–4089 (2018)
https://doi.org/10.1007/s00707-018-2223-2

ORIGINAL PAPER

S. Srividhya · K. Basant · R. K. Gupta · A. Rajagopal · J. N. Reddy

Influence of the homogenization scheme on the bending response of functionally graded plates

Received: 25 December 2017 / Revised: 6 February 2018 / Published online: 27 July 2018
© Springer-Verlag GmbH Austria, part of Springer Nature 2018

Abstract Functionally graded materials (FGM) are an advanced class of engineering composites constituting of two or more distinct phase materials described by continuous and smooth varying composition of material properties in the required direction. In this work, the effect of the material homogenization scheme on the flexural response of a thin to moderately thick FGM plate is studied. The plate is subjected to different loading and boundary conditions. The formulation is developed based on the first-order shear deformation theory. The mechanical properties are assumed to vary continuously through the thickness of the plate and obey a power-law distribution of the volume fraction of the constituents. The variation of volume fraction through the thickness is computed using two different homogenization techniques, namely rule of mixtures and Mori–Tanaka scheme. Comparative studies have been carried out to demonstrate the efficiency of the present formulation. The results obtained from the two techniques have been compared with the analytical solutions available in the literature. In addition to the above a parametric study bringing out the effect of boundary conditions, loads, and power-law index has also been presented.

1 Introduction

Many industrial and engineering materials as well as the majority of the "natural" materials are inhomogeneous, that is, they consist of dissimilar constituents (or phases) that are distinguishable at some (small) length scale. Each constituent shows different material properties and material orientations and may be inhomogeneous at some smaller length scale(s). Functionally graded materials are one of the typical examples of inhomogeneous materials at the macroscopic level in addition to composites, concrete, polycrystalline materials, and so on. Composite materials have been successfully used in many engineering and civilian applications for many years because of their excellent strength to weight and stiffness to weight ratios. Functionally graded materials (FGM) are a special class of composites in which the volume fractions of two or more materials are varied continuously as a function of position along certain dimension(s) (often, through thickness) of the structure to achieve a required functionality. A typical FGM, with a high bending–stretching coupling effect, is an inhomogeneous composite made from different phases of material constituents (e.g., ceramic and metal for thermal barrier structures). A representation of such a material is shown in Fig. 1 [1,2], where spherical or

K. Basant · R. K. Gupta
Advanced Systems Laboratory, DRDO, Hyderabad, India

S. Srividhya · A. Rajagopal
Department of Civil Engineering, Indian Institute of Technology Hyderabad, Kandi, Sangareddy, Telangana, India

J. N. Reddy (✉)
Department of Mechanical Engineering, Texas A & M University, College Station, TX, USA
E-mail: jnreddy@tamu.edu

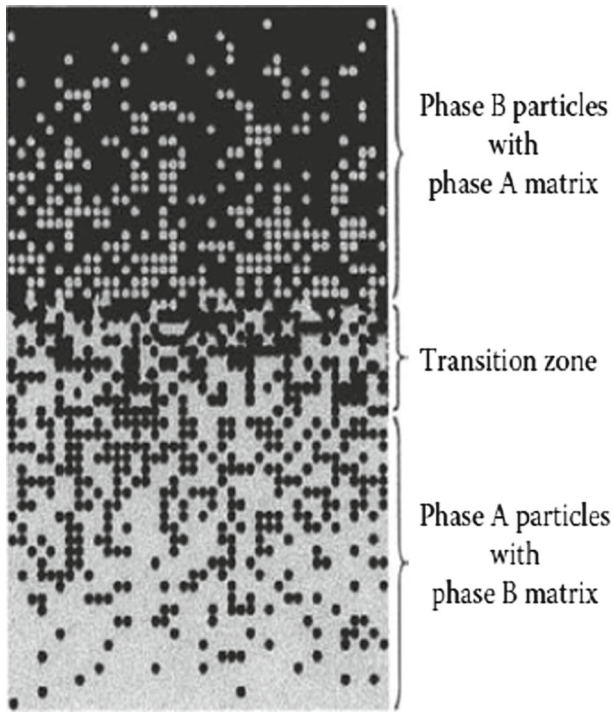

Fig. 1 An FGM with the volume fractions of constituent phases graded in one (vertical) direction [1,2]

nearly spherical particles are embedded within an isotropic matrix. The different microstructural phases in FGMs have different functions, and the overall FGMs attain the multistructural status from the gradation of their properties. FGMs have shown promise and potential applications, which are both numerous and diverse (e.g., biomedical, optoelectronic, spacecrafts, chemical, mechanical and other engineering applications [2–4]). Due to smooth and continuous variation of the material properties from one surface to the other, FGMs are usually superior to the conventional composite materials in mechanical behavior due to diffuse interface (i.e., no abrupt change in the material). FGMs possess a number of advantages such as improved residual stress distribution, enhanced thermal properties, higher fracture toughness and reduced stress intensity factors, and high wear resistance, among others. Therefore, the knowledge of the deformation and stress variations is of much practical importance for the optimal design of FGMs in structural applications involving bending and stretching.

A primary task in mechanics of materials is the prediction of the material's behavior. This requires the estimation of the effective (overall) properties of the composition, commonly known as the homogenization. When the precise information about the size, shape and the distribution of phases is not available, the effective elastic moduli of the graded microstructures must be evaluated based on the volume fraction distribution and the approximate shape of the dispersed phase. Several micromechanical models have been developed over the years to infer the effective properties of macroscopically homogeneous composites and graded composite materials like FGMs. References [3,5–8] have discussed in detail the various models used and made a comparison of estimated properties obtained from them. The comparisons [6] show that there is a variation in the estimated properties with different models to the tune of 7–30% for a stiffness ratios of 2–5.

Rule of mixtures (Voigt model), the most popular and largely used model to estimate the through-thickness properties of FGMs [9,10], Hashin–Shtrikman bounds, also called the composite sphere assemblage model [11,12], Mori–Tanaka homogenization scheme [5,13–15], and self-consistent schemes [11,16–18] have been reported in the literature and used for the determination of the bounds for the effective properties of heterogeneous materials like composites and FGM's. Comparisons have been made with the models with references to the self-consistent scheme. The comparison of the results obtained with analytical solutions or experimental results is scant. There is also dearth of experimental results for FGM plates in the open literature probably because fabrication techniques are not adequately matured or the cost is high. References obtained from open literature show that the Voigt and the Mori–Tanaka schemes have been generally adopted for a study of FGM plate structures by most of the researchers [4,9,13,19–22], to name a few.

Considering either Voigt model or Mori–Tanaka scheme, researchers have attempted to study the bending behavior of FGM plates based on 3D elasticity solutions [9,13,23,24]. All these works are limited to simply supported plates under sinusoidal transverse mechanical or thermal loading. Reddy and Cheng [24] and Vel and Batra [13] have accounted for the variation of material properties through the thickness according to a power-law distribution and the locally effective material properties obtained in terms of the volume fractions of the constituents by the Mori–Tanaka scheme. Kashtalyan [25] derived the elasticity solutions making use of the Plevako general solution of the equilibrium equations for inhomogeneous isotropic media. Elishakoff and Gentilini [26] carried out a 3D analysis of clamped functionally graded plates under uniformly distributed load applying the Ritz energy method. It is observed from all these works that the membrane stress variation through the thickness does not necessarily lie between the values of pure ceramic and metallic plates for the simply supported FGM plates. A similar conclusion is also drawn for the clamped FGM plates under mechanical loads.

Vast literature is available on the thermo-elastic buckling and vibration analysis of functionally graded material beams and plates [9,13,23,24,27]. These works are mainly focused on parametric effects of the power-law index or other parameters of the models on the response of FGM beams and plates. Moreover, it has been observed that the material homogenization technique used by many of the researchers has been rule of mixtures with power-law, but only a few attempted a comparison of the rule of mixture (RM) with the Mori–Tanaka scheme (MT). In particular, there are no extensive studies in the literature that report the influence of various homogenization schemes on the bending response of FGM plates. The primary objective of this study is to fill this gap in the literature.

In this study, bending analyses of FGM plates have been carried out to have a good understanding of the influence of a homogenization scheme (effective material properties through the thickness) on the deflections and stresses. The first-order shear deformation theory and the finite element method are used to develop the computational model of the plate bending problem. Two homogenization schemes, namely, the rule of mixtures and the Mori–Tanaka scheme, have been used for estimating the effective properties. The material properties of the plate are considered to vary according to a power-law distribution across the thickness of the plate. To obtain the exact material property at any point, a quadrature rule with higher integration points has to be used. A comparison of the results obtained with the two schemes is discussed in detail. A parametric study with different loading parameters has been carried out simulating the effect of aspect ratio of the plate and boundary conditions. The formulation is validated by comparing the present results with those available in the literature for simply supported square plates under distributed transverse load. In particular, since experimental results are not available, displacements, strains, and stresses obtained from the two schemes are compared with the exact solutions obtained by Zenkour [28] for simply supported plates. Numerical results are provided to show the effect of the boundary conditions and power-law index on the deformations and stresses of the FGM plates with various boundary conditions.

2 Estimation of effective moduli for two-phase composites

2.1 The Mori–Tanaka scheme

The Mori–Tanaka scheme for estimating the effective moduli is applicable to regions of the graded microstructure that have a well-defined continuous matrix and a discontinuous particulate phase, see Fig. 2a [13]. It takes into account the interaction of the elastic fields between neighboring inclusions. It is assumed that the matrix phase, denoted by the subscript m, is reinforced by spherical particles of a particulate phase, denoted by the subscript c.

Mori and Tanaka [5,14] derived a method to calculate the average internal stress in the matrix of a material. It was reformulated by Benveniste [15] for use in the computation of the effective properties of composite materials. According to the Mori–Tanaka scheme the effective elastic properties of the FGM can be expressed as:

$$\frac{K - K_c}{K_m - K_c} = \frac{V_m}{1 + (1 - V_m)\dfrac{K_m - K_c}{K_c + \dfrac{4}{3}G_c}},$$

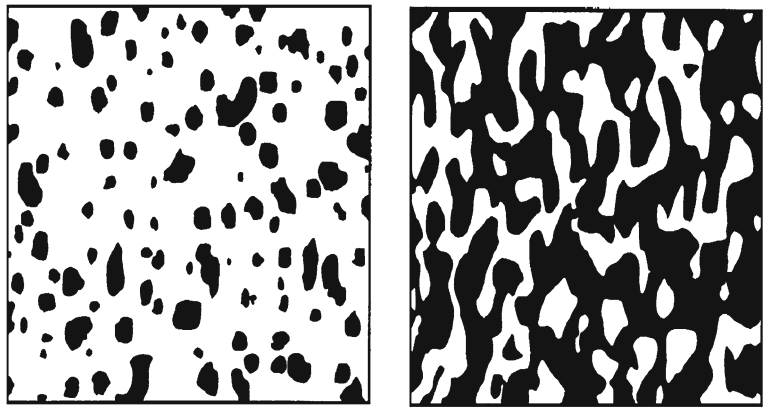

Fig. 2 Two-phase material with **a** particulate microstructure and **b** skeletal microstructure [13]

$$\frac{G - G_c}{G_m - G_c} = \frac{V_m}{1 + (1 - V_m)\dfrac{(G_m - G_c)}{G_c + f_c}} \tag{1}$$

where

$$f_c = \frac{G_c(9K_c + 8G_c)}{6(K_c + 2G_c)} \tag{2}$$

in which K and G are bulk modulus and shear modulus, respectively. The subscripts c and m refer to ceramic and metal phases, respectively. The above estimates for the effective local bulk modulus K and shear modulus G are useful for a random distribution of isotropic particles in an isotropic matrix. We note that K and G are related to Young's modulus and Poisson's ratio ν by the following equations:

$$E = \frac{9KG}{3K + G}, \qquad \nu = \frac{3K - 2G}{2(3K + G)} \tag{3}$$

2.2 The Voigt model: the rule of mixtures

This method assumes that each reinforcement inclusion is embedded in a continuum material whose effective properties are those of the composite [1,13]. This method does not distinguish between matrix and reinforcement phases, and the same overall moduli are predicted in another composite in which the roles of the phases are interchanged. This makes it particularly suitable for determining the effective moduli in those regions that have an interconnected skeletal microstructure as shown in Fig. 2b. The Voigt model has been adopted in most analyses of FGM structures [9,13,19,23,24,29–32]. The advantage of using the rule of mixture is the simplicity of implementation and the ease of computation. The properties emanating from this model can be considered as the upper and the lower bounds for the effective elastic properties of a heterogeneous material. The effective material properties P_f of the FGM layer can be expressed as

$$P_f = \sum_{j=1}^{n} P_j V_{fj} \tag{4}$$

where P_j and V_{fj} are the material properties and volume fraction of the constituent material j, and the sum of the volume fractions of all the constituent materials is given by

$$\sum_{j=1}^{n} V_{fj} = 1. \tag{5}$$

3 Theoretical formulations

3.1 Introduction

The first-order shear deformation theory (FSDT) accounts for the transverse shear strains as a constant through the plate thickness and hence requires a shear correction factor to estimate the transverse shear forces as shown by Reddy et al. [10,27,33,34]. Here we develop equations of motion of functionally graded plates based on the FSDT.

Consider a plate of total thickness h and composed of functionally graded material through the thickness. It is assumed that the material is isotropic, and the grading is assumed to be only through the thickness. The xy-plane is taken to be the undeformed mid-plane of the plate with the z-axis positive downward from the mid-plane. Further, we restrict the formulation to linear elastic material behavior, small strains and displacements. The variation of the properties through the thickness is considered to be either exponential (called E-FGM) or based on a power series (called P-FGM) in the literature, which covers most of the existing analytical models. The power-law is most popular because of its simplicity and algebraic nature which is easy to implement. The volume fraction of the ceramic at any distance from the mid-plane can be expressed in the form of a power-law as:

$$V_{\mathrm{c}} = \left(\frac{1}{2} + \frac{z}{h}\right)^n \tag{6.1}$$

where n is the power-law index which varies from 0 to ∞.

Considering Eqs. 4–6, the material property at any z using the power-law can be expressed as:

$$E(z) = [E_{\mathrm{c}} - E_{\mathrm{m}}]\left(\frac{1}{2} + \frac{z}{h}\right)^n + E_{\mathrm{m}} \tag{6.2}$$

where E_{c} and E_{m} are the elastic modulus of ceramic and metal, respectively.

3.2 Displacement fields and strains

Based on the first-order shear deformable plate theory [10], the in-plane displacement u and v at any point along the x- and y-axes can be expressed in terms of the mid-plane displacements u_0, v_0 and rotations ϕ_x and ϕ_y as

$$u(x, y, z) = u_0(x, y) + z\phi_x(x, y), \tag{7}$$

$$v(x, y, z) = v_0(x, y) + z\phi_y(x, y), \tag{8}$$

$$w(x, y, z) = w_0(x, y) \tag{9}$$

where ϕ_x and ϕ_y are rotations of the mid-plane about y- and x-axes, respectively. The transverse displacement w along the z-axis is assumed to be constant through the thickness. The in-plane strain–displacement relations can be expressed as

$$\begin{Bmatrix} \varepsilon_{xx} \\ \varepsilon_{yy} \\ \gamma_{xy} \end{Bmatrix} = \begin{Bmatrix} \dfrac{\partial u_0}{\partial x} \\ \dfrac{\partial v_0}{\partial y} \\ \dfrac{\partial u_0}{\partial y} + \dfrac{\partial v_0}{\partial x} \end{Bmatrix} + z \begin{Bmatrix} \dfrac{\partial \phi_x}{\partial x} \\ \dfrac{\partial \phi_y}{\partial y} \\ \dfrac{\partial \phi_x}{\partial y} + \dfrac{\partial \phi_y}{\partial x} \end{Bmatrix}, \tag{10}$$

and the transverse shear strains are given by

$$\gamma_{xz} = \phi_x + \frac{\partial w}{dx}, \tag{11}$$

$$\gamma_{yz} = \phi_y + \frac{\partial w}{dy}. \tag{12}$$

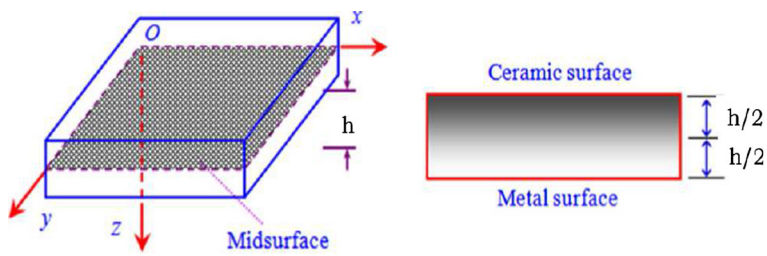

Fig. 3 Schematic representation of a functionally graded plate

3.3 Constitutive relations

Let us consider the case of a rectangular plate of length a, breadth b, and total height h with the coordinate system as shown in Fig. 3. Here we assume that the material property gradation is through the thickness, and the volume fraction variation is represented by the power-law as shown in Eq. (6.1).

The effective properties of the graded structure are estimated by both rule of mixtures shown in Eq. (4) and Mori–Tanaka scheme as shown in Eq. (3). Here we assume that the elastic moduli E vary according to Eqs. (3) and (4). Poisson's ratio ν is assumed to be a constant. Assuming plane stress condition, the in-plane stress–strain relations are

$$\begin{Bmatrix} \sigma_{xx} \\ \sigma_{yy} \\ \sigma_{xy} \end{Bmatrix} = \frac{E(z)}{1-\nu^2} \begin{bmatrix} 1 & \nu & 0 \\ \nu & 1 & 0 \\ 0 & 0 & \dfrac{1-\nu}{2} \end{bmatrix} \begin{Bmatrix} \varepsilon_{xx} \\ \varepsilon_{yy} \\ \gamma_{xy} \end{Bmatrix}. \tag{13}$$

The transverse shear stress–strain relations are

$$\begin{Bmatrix} \sigma_{yz} \\ \sigma_{xz} \end{Bmatrix} = \begin{bmatrix} G(z) & 0 \\ 0 & G(z) \end{bmatrix} \begin{Bmatrix} \gamma_{yz} \\ \gamma_{xz} \end{Bmatrix} \tag{14}$$

where the shear modulus $G(z)$ can be expressed in terms of Young's modulus and Poisson's ratio of ceramic and metal. The stress and moment resultants are

$$\begin{aligned} \begin{Bmatrix} N_{xx} \\ N_{yy} \\ N_{xy} \end{Bmatrix} &= \int_{-h/2}^{h/2} \begin{Bmatrix} \sigma_{xx} \\ \sigma_{yy} \\ \sigma_{xy} \end{Bmatrix} \mathrm{d}z, \\ \begin{Bmatrix} M_{xx} \\ M_{yy} \\ M_{xy} \end{Bmatrix} &= \int_{-h/2}^{h/2} \begin{Bmatrix} \sigma_{xx} \\ \sigma_{yy} \\ \sigma_{xy} \end{Bmatrix} z\mathrm{d}z, \\ \begin{Bmatrix} Q_{yz} \\ Q_{xz} \end{Bmatrix} &= \kappa_{\mathrm{s}} \int_{-h/2}^{h/2} \begin{Bmatrix} \sigma_{yz} \\ \sigma_{xz} \end{Bmatrix} \mathrm{d}z \end{aligned} \tag{15}$$

where N_{xx}, N_{yy}, and N_{xy} are the in-plane stress resultants and M_{xx}, M_{yy}, and M_{xy} are the moment resultants. The transverse shear stress resultants are given by Q_{xz} and Q_{yz}. A value of 5/6 is assumed for the shear energy correction factor κ_{s} [34,35].

3.3.1 Shear correction factor

The transverse shear strains shown in Eqs. (11) and (12) are constant through the thickness, and hence, it also implies that the transverse shear stresses will also be constant. From the elementary theory of homogeneous beams the transverse stress distribution has been shown to be parabolic. The discrepancy in the actual stress state as obtained from the exact solutions and the constant stress state as predicted by FSDT needs to be corrected to maintain the energy balance. This is done by multiplying the integrals in Eq. (15) by a parameter κ_{s} while computing the shear force resultants. The parameter κ_{s} is called the shear correction coefficient or factor. The shear correction factor is computed such that strain energy due to transverse shear stresses in Eq. (15) equals the strain energy due to the true transverse stresses predicted by the 3D elasticity theory. The shear

correction factor is the ratio of the strain energy associated with FSDT to the 3D elasticity theory. The value in general depends on the geometry and the material properties of the plate. A detailed explanation is provided by Cowper [35] on the shear correction factor, wherein he has derived the formulas for different cross sections as a function of Poisson's ratio. For a rectangular cross section $\kappa_s = \dfrac{10(1+\nu)}{12+11\nu}$.

3.4 Governing equations

The equations of equilibrium for the bending of plates based on the first-order shear deformable plate theory are

$$\begin{aligned}
&\frac{\partial N_{xx}}{\partial x} + \frac{\partial N_{xy}}{\partial y} = 0,\\
&\frac{\partial N_{xy}}{\partial x} + \frac{\partial N_{yy}}{\partial y} = 0,\\
&\frac{\partial Q_{yz}}{\partial x} + \frac{\partial Q_{xz}}{\partial y} + q = 0,\\
&\frac{\partial M_{xx}}{\partial x} + \frac{\partial M_{xy}}{\partial y} - Q_x = 0,\\
&\frac{\partial M_{xy}}{\partial x} + \frac{\partial M_{yy}}{\partial y} - Q_y = 0.
\end{aligned} \tag{16}$$

3.5 Finite element formulation

3.5.1 Element description

A C^0 continuous, isoparametric, 4-node element based on first-order shear deformable plate theory with 5 degrees of freedom u, v, w, ϕ_x, ϕ_y and Lagrange interpolation function (N_i) is used in the finite element analysis:

$$\begin{aligned}
u &= \sum_{i=1}^{4} N_i\,(\xi,\eta) u_i,\\
v &= \sum_{i=1}^{4} N_i\,(\xi,\eta) v_i,\\
w &= \sum_{i=1}^{4} N_i\,(\xi,\eta) w_i,\\
\phi_x &= \sum_{i=1}^{4} N_i\,(\xi,\eta) (\phi_x)_i,\\
\phi_y &= \sum_{i=1}^{4} N_i\,(\xi,\eta) \left(\phi_y\right)_i.
\end{aligned} \tag{17}$$

3.5.2 Element stiffness matrix

The strain energy for the bending of shear deformable FGM plates is given by

$$U = \frac{1}{2}\int_V \{\sigma\}^{\mathrm{T}}\{\varepsilon\}\,\mathrm{d}V + \frac{\kappa_s}{2}\int_V \{\sigma_s\}^{\mathrm{T}}\{\varepsilon_s\}\,\mathrm{d}V. \tag{18}$$

The in-plane stresses and strains are given by

$$\begin{aligned}
\{\sigma\} &= \left\{\sigma_{xx} \quad \sigma_{yy}\ \sigma_{xy}\right\}^{\mathrm{T}},\\
\{\varepsilon\} &= \left\{\varepsilon_{xx} \quad \varepsilon_{yy}\ \gamma_{xy}\right\}^{\mathrm{T}}.
\end{aligned} \tag{19}$$

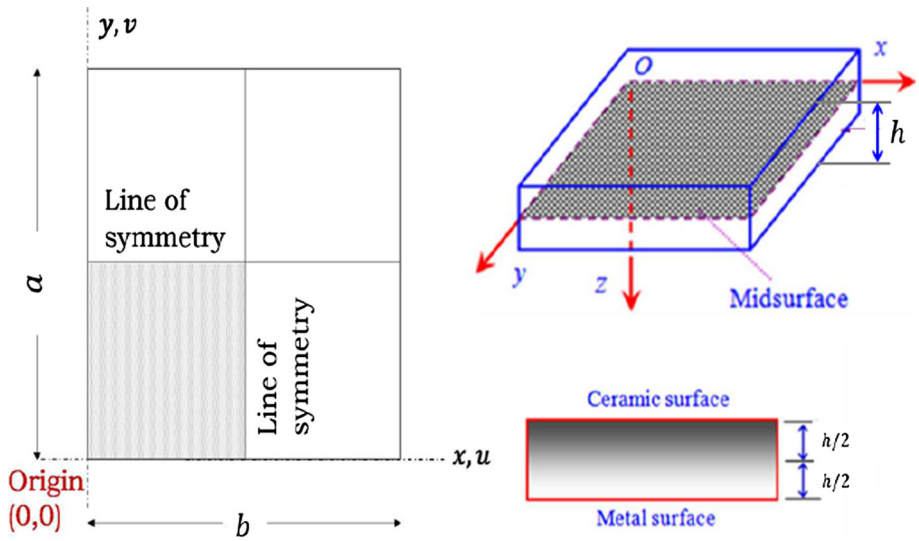

Fig. 4 Geometric details of the square plate with quarter symmetry and axes convention followed

Table 1 Material properties used for the study

Property	Young's modulus, E (GPa)	Poisson's ratio, ν
Alumina	380	0.3
Aluminum	70	0.3

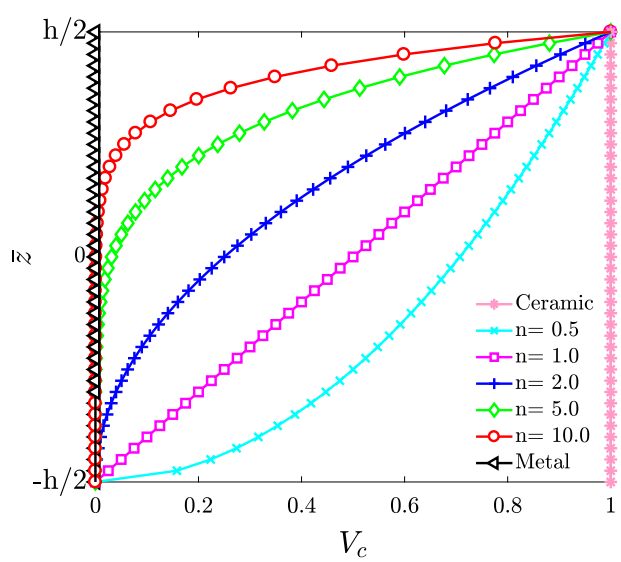

Fig. 5 Through the thickness variation of volume fraction of the ceramic material based on power-law distribution

The shear stresses and strains are given by

$$\{\sigma_s\} = \left\{ \sigma_{yz} \ \sigma_{xz} \right\}^T, \\ \{\varepsilon_s\} = \left\{ \gamma_{yz} \ \gamma_{xz} \right\}^T. \tag{20}$$

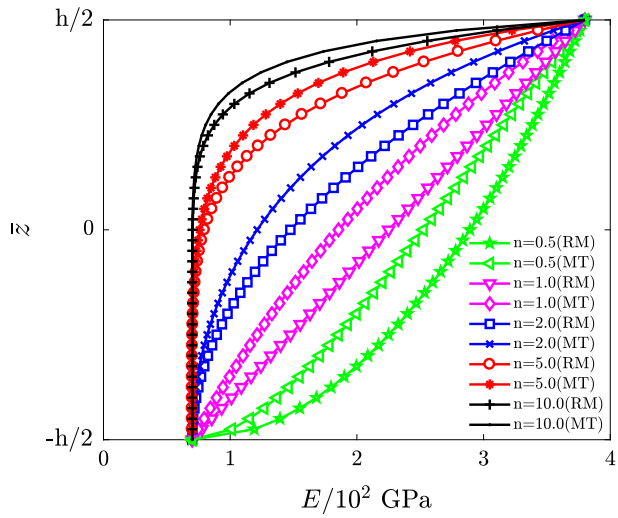

Fig. 6 Comparison of Young's modulus through the thickness of the FGM plate with rule of mixture and Mori–Tanaka scheme

By using the constitutive and kinematic equations and nodal degrees of freedom, the element stiffness matrix can be obtained using the principle of minimum potential energy as

$$\left[K^e\right] = \int_{\Omega^e} \left[\int_{-h/2}^{h/2} [B]^{\mathrm{T}} [D] [B] \, \mathrm{d}z \right] \mathrm{d}\Omega + \kappa_s h \int_{\Omega^e} \left[\int_{-h/2}^{h/2} [B_s]^{\mathrm{T}} [D_s] [B_s] \, \mathrm{d}z \right] \mathrm{d}\Omega \tag{21}$$

where $[B]$ and $[B_s]$ relate in-plane and shear strains to the degree of freedom matrix, and $[D]$ and $[D_s]$ are the constitutive equations which relate the in-plane stresses and transverse shear stresses to the corresponding strains, respectively. The bending term in the element stiffness matrix is integrated using (2×2) rule. Reduced integration (1×1) is used for the shear term to avoid shear locking. The finite element system of equations is

$$[K]\{\Delta\} = \{F\} \tag{22}$$

where $[K]$, $\{\Delta\}$, and $\{F\}$ are the assembled stiffness matrix, nodal displacement vector, and load vector.

3.6 Numerical integration

In the present work, numerical integration technique has been implemented to evaluate the integrals for finding the material properties of the FGM plate using a power-law distribution. Adopting numerical integration is easier, if we are trying to automate the finite element code. The sum of these integrand values multiplied by appropriate weights (called Gauss weights) gives an approximation to the integral.

$$I = \int_{-1}^{1} P_f(z) \mathrm{d}z \approx \sum_{i=1}^{n} w_i P_f(z_i) \tag{23}$$

where z_i: Gauss points; n: total number of Gauss points; w_i: Gauss weights; $P_f(z_i)$: value of the integrand at the Gauss point z_i.

Using this method it is easy to find the variation of the material properties along the thickness of the plate at any point. It is simpler to implement and also faster than symbolic integration in this case. To have an effective estimate of the material property at any point, a quadrature rule with larger number of integration points needs to be employed.

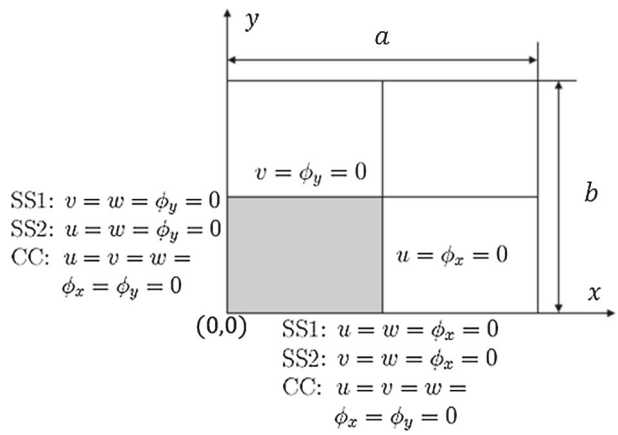

Fig. 7 Different types of boundary conditions

Table 2 Non-dimensional center deflections of the FGM plate with SS1 boundary condition for various mesh sizes and a/h ratio

a/h	Mesh size	n					
		Ceramic	0.2	0.5	1	2	Metal
20	2 × 2	0.4354	0.5309	0.6713	0.8729	1.1187	2.3637
	4 × 4	0.4431	0.5403	0.6833	0.8885	1.1387	2.4056
	6 × 6	0.4444	0.5419	0.6850	0.8908	1.1418	2.4122
	8 × 8S	0.4444	0.5419	0.6852	0.8910	1.1419	2.4124
	8 × 8F	0.2575	0.3070	0.3774	0.4783	0.6166	1.3980
	8 × 8R	0.1114	0.1359	0.1718	0.2234	0.2864	0.6050
	16 × 16	0.4444	0.5419	0.6852	0.8910	1.1419	2.4124
10	2 × 2	0.4404	0.5367	0.6782	0.8814	1.1297	2.3908
	4 × 4	0.4477	0.5456	0.6895	0.8961	1.1486	2.4302
	6 × 6	0.4489	0.5471	0.6914	0.8986	1.1517	2.4367
	8 × 8S	0.4489	0.5471	0.6916	0.8988	1.1520	2.4368
	8 × 8F	0.3727	0.4500	0.5621	0.7226	0.9286	2.0233
	8 × 8R	0.1126	0.1372	0.1734	0.2253	0.2888	0.6110
	16 × 16	0.4489	0.5471	0.6916	0.8988	1.1520	2.4368
5	2 × 2	0.4594	0.5587	0.7043	0.9134	1.1713	2.4940
	4 × 4	0.4649	0.5656	0.7132	0.9253	1.1864	2.5239
	6 × 6	0.4659	0.5667	0.7147	0.9272	1.1889	2.5289
	8 × 8S	0.4659	0.5667	0.7148	0.9273	1.1889	2.5289
	8 × 8F	0.4425	0.5368	0.6746	0.8722	1.1192	2.4024
	8 × 8R	0.1168	0.1421	0.1792	0.2325	0.2981	0.6340
	16 × 16	0.4659	0.5667	0.7148	0.9273	1.1889	2.5289

S selective integration, *F* full integration, *R* reduced integration

4 Results and discussion

The bending behavior of a square FGM plate comprised of aluminum/alumina under distributed transverse load is taken up for investigation. The top surface of the FGM plate is ceramic (alumina) rich, and the bottom surface is pure metal (aluminum). A schematic model of the FGM plate and its sign convention is shown in Fig. 4. The datum has been considered at the mid-plane which is also the geometric mid-surface of the plate. To reduce the problem size and owing to symmetry in geometry and boundary conditions, a quarter plate has been considered for analysis. The material properties assumed in the study are tabulated in Table 1.

The variation of the volume fraction of ceramic V_c is obtained from Eq. (6), and the effective Young's modulus E in the thickness direction of the FGM plate is obtained from Eqs. (3) and (4). The variation is depicted in Figs. 5 and 6 for different values of the power-law index n. It is observed that the effective Young's modulus E changes continuously from top surface to bottom surface except for the extreme cases such as $n = 0$ and $n = \infty$, for which it is constant.

It is also observed that for any given distance from the mid-plane the effective Young's modulus obtained from the rule of mixture is larger than that obtained from the Mori–Tanaka scheme. This implies that the

Table 3 Comparison of non-dimensional center deflections and stresses with analytical solution under sinusoidal load, $a/h = 10$

n	$\bar{w}$	$\bar{\sigma}_{xx}$	$\bar{\sigma}_{yy}$	$\bar{\sigma}_{xy}$
Ceramic				
Present				
RM	0.2839	1.9572	1.3048	0.7026
MT	0.2839	1.9572	1.3048	0.7026
Zenkour [28]				
RM	0.2960	1.9955	1.3121	0.7065
1				
Present				
RM	0.5683	3.0249	1.4827	0.6067
MT	0.6341	3.2676	1.4198	0.5935
Zenkour [28]				
RM	0.5889	3.0870	1.4894	0.6110
2				
Present				
RM	0.7284	3.5321	1.3924	0.5408
MT	0.7795	3.7780	1.2731	0.5542
Zenkour [28]				
RM	0.7573	3.6094	1.3954	0.5441
3				
Present				
RM	0.8010	3.7857	1.2751	0.5495
MT	0.8427	4.0752	1.1538	0.5637
Zenkour [28]				
RM	0.8377	3.8742	1.2748	0.5525
5				
Present				
RM	0.8636	4.1454	1.1071	0.5728
MT	0.9068	4.5522	1.0084	0.5810
Zenkour [28]				
RM	0.9118	4.2488	1.1029	0.5755
10				
Present				
RM	0.9500	4.9701	0.8823	0.5870
MT	1.0084	5.5454	0.8546	0.5963
Zenkour [28]				
RM	1.0089	5.0890	0.8775	0.5894
Metal				
Present				
RM	1.5414	1.9572	1.3048	0.7026
MT	1.5414	1.9572	1.3048	0.7026
Zenkour [28]				
RM	1.6070	1.9955	1.3121	0.7065

stiffness as exhibited by the rule of mixture shall be larger than that of Mori–Tanaka. Hence, the results from Mori–Tanaka should exhibit larger deflections.

4.1 Loads and boundary conditions

A transverse force in the form of uniformly distributed load (UDL) and sinusoidal loads (SSL) has been applied on the FGM plate under consideration. Figure 7 depicts the boundary conditions used for the analysis for each case. Uniformly distributed load has been applied as $q(x, y) = q_o$, and the sinusoidal load takes the form of $q(x, y) = q_o \sin(\pi x/a) \sin(\pi y/b)$. The following non-dimensional quantities are considered in the forthcoming examples:

$$\bar{w} = \frac{10h^3 E_c}{a^4 q_0} w\left(\frac{a}{2}, \frac{b}{2}\right), \quad \bar{z} = \frac{z}{h}, \quad \bar{\sigma}_{xx} = \frac{h}{q_o a}\sigma_{xx}\left(\frac{a}{2}, \frac{b}{2}, \frac{h}{2}\right),$$
$$\bar{\sigma}_{yy} = \frac{h}{q_o a}\sigma_{yy}\left(\frac{a}{2}, \frac{b}{2}, \frac{h}{3}\right), \quad \bar{\sigma}_{xy} = \frac{h}{q_o a}\sigma_{xy}\left(0, 0, \frac{-h}{3}\right), \quad \bar{\sigma}_{xz} = \frac{h}{q_o a}\sigma_{xz}\left(0, \frac{b}{2}, 0\right).$$

Table 4 Comparison of non-dimensional center deflections and stresses with analytical solution under uniformly distributed load, $a/h = 10$

n	$\bar{w}$	$\bar{\sigma}_{xx}$	$\bar{\sigma}_{yy}$	$\bar{\sigma}_{xy}$
Ceramic				
Present				
RM	0.4493	2.8621	1.9081	1.2628
MT	0.4493	2.8621	1.9081	1.2628
Zenkour [28]				
RM	0.4665	2.8932	1.9103	1.2850
1				
Present				
RM	0.8994	4.4236	2.1683	1.0905
MT	1.0035	4.7785	2.0763	1.0667
Zenkour [28]				
RM	0.9287	4.4745	2.1692	1.1143
2				
Present				
RM	1.1528	5.1653	2.0363	0.9719
MT	1.2335	5.5249	1.8618	0.9961
Zenkour [28]				
RM	1.1940	5.2296	2.0338	0.9907
3				
Present				
RM	1.2676	5.5362	1.8647	0.9877
MT	1.3335	5.9595	1.6873	1.0131
Zenkour [28]				
RM	1.3200	5.6108	1.8593	1.0047
5				
Present				
RM	1.3664	6.0622	1.6190	1.0296
MT	1.4347	6.6571	1.4747	1.0442
Zenkour [28]				
RM	1.4356	6.1504	1.6104	1.0451
10				
Present				
RM	1.5029	7.2682	1.2903	1.0550
MT	1.5953	8.1095	1.2498	1.0718
Zenkour [28]				
RM	1.5876	7.3689	1.2820	1.0694
Metal				
Present				
RM	2.4389	2.8621	1.9081	1.2628
MT	2.4389	2.8621	1.9081	1.2628
Zenkour [28]				
RM	2.5327	2.8932	1.9103	1.2850

The efficacy of the present formulation is assessed by studying a simply supported square FGM plate under distributed load q_0. The non-dimensional center displacements for different mesh sizes, thickness ratios and varying power-law index are tabulated in Table 2. It is observed that the results become consistent beyond a mesh size of 8×8. Hence, a mesh size of 8×8 has been used for further studies. To avoid shear locking selective integration is used, i.e., 2×2 rule for bending terms and 1×1 rule for shear terms. The results for different mesh sizes have also been tabulated. The results compare well with those in the literature [28,36,37].

The non-dimensional center deflections and stresses are compared with the results obtained from the analytical solution by Zenkour [28], and they agree well under two types of loading conditions (SSL and UDL), as presented in Tables 3 and 4. Zenkour [28] employed the rule of mixtures to find the effective properties of the FGM plate with HSDT (sinusoidal shear deformation theory), and those results have been compared with the present rule of mixtures results and Mori–Tanaka. The results obtained from Mori–Tanaka scheme give slightly higher values.

Figures 8 and 9 show the variation of center deflections with variation in the power-law index. It is observed that for lower power-law index ($n = 0$), the present results from rule of mixture match closely with the analytical solutions as given by [28], but deviate as the value of n increases. It is also observed that the curve matches very well with the results obtained from Mori–Tanaka scheme for higher values of the power-law index. This

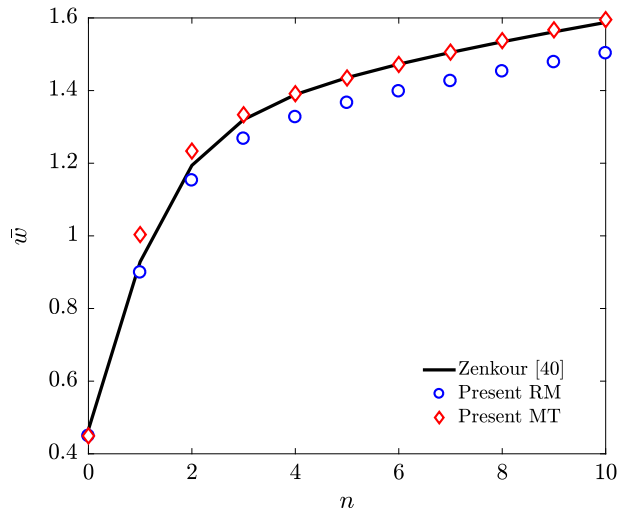

Fig. 8 Comparison of center deflections obtained from RM and MT with Zenkour [28] under UDL ($a/h = 10$, SS1 BC)

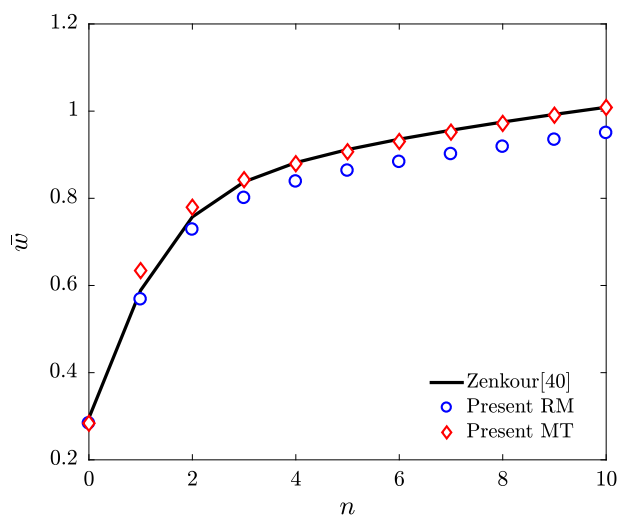

Fig. 9 Comparison of center deflections obtained from RM and MT with Zenkour [28] under SSL ($a/h = 10$, SS1 BC)

is observed for both the cases of UDL and SSL. A very important conclusion can be made from the above graphs that the rule of mixtures gives correct estimates of the elastic properties for lower power-law index (n), and Mori–Tanaka scheme is well suited to estimate and predict the effective properties with higher power-law index. So the choice of homogenization scheme should be based on the requirements of gradation in the FGM. It can also be concluded that Mori–Tanaka scheme is better suited to model steep gradients and shall give better estimates of effective properties, whereas the rule of mixtures provides a conservative estimate of the effective properties, and this is one reason why numerous researchers have used rule of mixtures for their study.

In Table 5 the non-dimensional center deflections and in-plane stresses (present FSDT) are compared with different theories by Neves et al. [36] and Carrera et al. [37]. The present FSDT stress results are closer to the HSDT results of Neves et al. [36]. This also reiterates the fact that FSDT may be suited well for simpler geometries and moderately thick plates. The effect of aspect ratio (a/h) and power-law index is observed from Tables 5, 6, and 7. With the increase in n value from 0 to ∞ the center deflections and the stresses increase in order. This is expected as $n = 0$ corresponds to pure ceramic ($E = 380$ GPa) and $n = \infty$ corresponds to pure metal ($E = 70$ GPa). It is clear from Tables 5, 6, and 7 that the deflection increases as the side-to thickness ratio (a/h) decreases. The effect of boundary conditions (SS1, SS2, and CC) on the deflections is shown. The effect of the boundary conditions (SS1, SS2, and CC) on the deflections is presented in Tables 6 and 7. It is observed that there is not much difference in deflection values for SS1 and SS2 boundary conditions, and they

Table 5 Comparison of non-dimensional center deflections under sinusoidal load

n	a/h	$\bar{\sigma}_{xx}(z = h/3)$			$\bar{w}$		
		4	10	100	4	10	100
1	Neves et al. CLPT [36]	0.8060	2.0150	20.1500	0.5623	0.5623	0.5623
	Neves et al. FSDT [36]	0.8060	2.0150	20.1500	0.7291	0.5889	0.5625
	Neves et al. HSDT [36]	0.5806	1.4874	14.9440	0.7308	0.5913	0.5648
	Carrera et al. [37]	0.7856	2.0068	20.1490	0.7289	0.5890	0.5625
	Present RM	0.5931	1.4827	14.8273	0.6034	0.5683	0.5612
	Present MT	0.5679	1.4198	14.1981	0.6715	0.6341	0.6263
4	Neves et al. CLPT [36]	0.6420	1.6049	16.0490	0.8281	0.8281	0.8281
	Neves et al. FSDT [36]	0.6420	1.6049	16.0490	1.1125	0.8736	0.8280
	Neves et al. HSDT [36]	0.4338	1.1592	11.7370	1.1552	0.8770	0.8241
	Carrera et al. [37]	0.5986	1.5874	16.0470	1.1673	0.8828	0.8286
	Present RM	0.4724	1.1810	11.8100	0.8968	0.8387	0.8266
	Present MT	0.4280	1.0699	10.6989	0.9429	0.8794	0.8662
10	Neves et al. CLPT [36]	0.4796	1.1990	11.9900	0.9354	0.9354	0.9354
	Neves et al. FSDT [36]	0.4796	1.1990	11.9900	1.3178	0.9966	0.9360
	Neves et al. HSDT [36]	0.3112	0.8468	8.6011	1.3760	0.9952	0.9228
	Carrera et al. [37]	0.4345	1.1807	11.9890	1.3925	1.0090	0.9361
	Present RM	0.3529	0.8823	8.8233	1.0282	0.9500	0.9338
	Present MT	0.3419	0.8546	8.5465	1.0913	1.0084	0.9912

are the same for the limiting cases corresponding to pure ceramic ($n = 0$) and pure metal ($n = \infty$). But for CC boundary condition there is a significant drop in the center deflections due to additional stiffness/rigidity which is also expected and well reported in the literature.

Two different material homogenization schemes have been considered for the analysis (rule of mixtures and Mori–Tanaka). The results for the non-dimensional center deflections using rule of mixtures and Mori–Tanaka scheme and percentage difference with respect to Mori–Tanaka solution are presented in Tables 6 and 7. It is observed that the non-dimensional center deflections as obtained by the Mori–Tanaka scheme are higher than those obtained from the rule of mixtures. This brings out the fact that the estimates of the mechanical properties through the thickness with Mori–Tanaka scheme are slightly lesser as compared to rule of mixtures. Also since rule of mixtures gives simply a weighted average of properties, the deflections are higher. The % difference is zero for the maximum and minimum cases and varying for intermediate values of power-law index n. The % difference is increasing up to $n = 1$ and then decreasing, and the same trend is observed for all cases with different a/h ratios and boundary conditions. The % difference is the same for any a/h ratio and loading condition, but varying by 1–2% between different boundary conditions. The maximum difference between the two schemes is observed at $n = 0.5$ in all the cases.

The non-dimensional deflections under uniformly distributed load using rule of mixtures and Mori–Tanaka scheme are plotted along the centerline of the plate for SS1 and CC boundary condition, as shown in Figs. 10 and 11. The results show that the deflections are zero at boundaries and increase to a maximum at the center of the plate. The difference in the deflections of rule of mixtures and Mori–Tanaka scheme is slightly higher in the case of Fig. 10 compared to Fig. 11. The variation of the non-dimensional in-plane stress ($\bar{\sigma}_{xx}$) through the thickness of the square FGM plate made up of (aluminum/alumina) under transverse distributed load has been studied, and the results are presented in Fig. 12. The Figure shows the variation of in-plane axial stress for uniformly distributed load using the rule of mixtures for different power-law index values through the thickness. It is observed that the through-thickness variation of in-plane axial stress is identical and linear for $n = 0$ and $n = \infty$ and becomes slightly nonlinear with increase in the power-law index value.

The variation of in-plane shear stress ($\bar{\sigma}_{xy}$) for different material homogenization schemes with a particular power-law index value $n = 0.5$ is shown in Fig. 13. The Mori–Tanaka scheme gives higher stress values at top and bottom. But in between both the homogenization rules give nearly the same values. Through-thickness variation of non-dimensional in-plane axial stress ($\bar{\sigma}_{xx}$) under uniformly distributed load and a particular power-law index value $n = 0.5$ with rule of mixture with two different boundary conditions (SS1 and CC) is shown in Fig. 14. It is observed that the in-plane axial stresses under SS1 type of boundary condition are higher than those of CC type of boundary conditions. Both the curves intersect at mid-plane and go to zero at the mid-height of the plate.

Table 6 Comparison of non-dimensional deflections for FGM plate subjected to sinusoidal load for a/h ratio, power-law index, and boundary conditions using RM and MT

a/h	BC's	n	0	0.5	1	2	∞
4	SS1	RM	0.3041	0.4650	0.6024	0.7727	1.6510
		MT	0.3041	0.5235	0.6715	0.8283	1.6510
		% Diff	0	11.2	10.3	6.7	0
	SS2	RM	0.3041	0.4483	0.5528	0.6759	1.6510
		MT	0.3041	0.4953	0.6069	0.7303	1.6510
		% Diff	0	9.5	8.9	7.5	0
	CC	RM	0.1263	0.1903	0.2449	0.3146	0.6854
		MT	0.1263	0.2131	0.2725	0.3386	0.6854
		% Diff	0	10.7	10.1	7.1	0
10	SS1	RM	0.2839	0.4373	0.5683	0.7284	1.5414
		MT	0.2839	0.4936	0.6341	0.7795	1.5414
		% Diff	0	11.4	10.4	6.6	0
	SS2	RM	0.2839	0.4206	0.5186	0.6314	1.5414
		MT	0.2839	0.4654	0.5694	0.6813	1.5414
		% Diff	0	9.6	8.9	7.3	0
	CC	RM	0.1040	0.1595	0.2070	0.2654	0.5644
		MT	0.1040	0.1799	0.2309	0.2843	0.5644
		% Diff	0	11.3	10.3	6.6	0
100	SS1	RM	0.2797	0.4315	0.5612	0.7192	1.5186
		MT	0.2797	0.4874	0.6263	0.7693	1.5186
		% Diff	0	11.5	10.4	6.5	0
	SS2	RM	0.2797	0.4149	0.5115	0.6222	1.5186
		MT	0.2797	0.4591	0.5616	0.6711	1.5186
		% Diff	0	9.6	8.9	7.3	0
	CC	RM	0.0991	0.1528	0.1987	0.2547	0.5378
		MT	0.0991	0.1726	0.2218	0.2724	0.5378
		% Diff	0	11.5	10.4	6.5	0

Table 7 Comparison of non-dimensional deflections for FGM plate subjected to uniformly distributed load for various a/h ratio, power-law index, and boundary conditions using RM and MT

a/h	BC's	n	0	0.5	1	2	∞
4	SS1	RM	0.4786	0.7323	0.9490	1.2171	2.5983
		MT	0.4786	0.8247	1.0580	1.3046	2.5983
		% Diff	0	11.2	10.3	6.7	0
	SS2	RM	0.4786	0.7041	0.8648	1.0529	2.5983
		MT	0.4786	0.7768	0.9484	1.1384	2.5983
		% Diff	0	9.4	8.8	7.5	0
	CC	RM	0.1775	0.2674	0.3440	0.4419	0.9638
		MT	0.1775	0.2993	0.3827	0.4756	0.9638
		% Diff	0	10.7	10.1	7.1	0
10	SS1	RM	0.4493	0.6920	0.8994	1.1528	2.4389
		MT	0.4493	0.7812	1.0035	1.2335	2.4389
		% Diff	0	11.4	10.4	6.5	0
	SS2	RM	0.4493	0.6637	0.8151	0.9883	2.4389
		MT	0.4493	0.7333	0.8939	1.0671	2.4389
		% Diff	0	9.5	8.8	7.4	0
	CC	RM	0.1451	0.2226	0.2888	0.3703	0.7876
		MT	0.1451	0.2509	0.3221	0.3967	0.7876
		% Diff	0	11.3	10.3	6.6	0
100	SS1	RM	0.4432	0.6836	0.8891	1.1394	2.4059
		MT	0.4432	0.7721	0.9922	1.2188	2.4059
		% Diff	0	11.5	10.4	6.5	0
	SS2	RM	0.4432	0.6554	0.8048	0.9749	2.4059
		MT	0.4432	0.7242	0.8825	1.0522	2.4059
		% Diff	0	9.5	8.8	7.3	0
	CC	RM	0.1379	0.2128	0.2767	0.3546	0.7488
		MT	0.1379	0.2403	0.3088	0.3793	0.7488
		% Diff	0	11.5	10.4	6.5	0

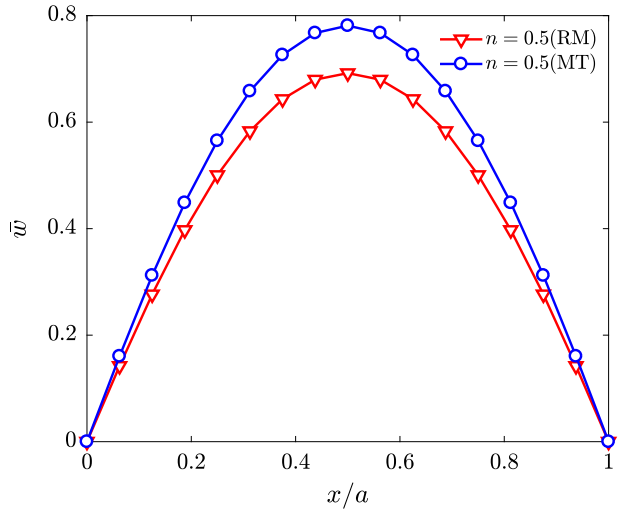

Fig. 10 Non-dimensional deflection along the centerline of the FGM plate under UDL using RM and MT ($a/h = 10$, SS1 BC)

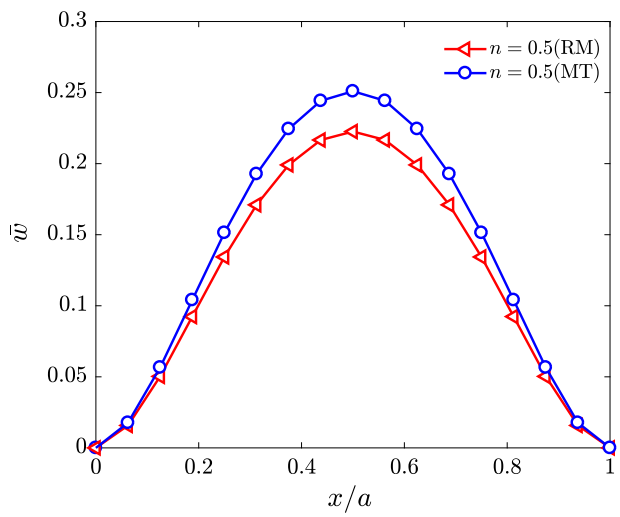

Fig. 11 Non-dimensional deflection along the centerline of the FGM plate under UDL using RM and MT ($a/h = 10$, CC BC)

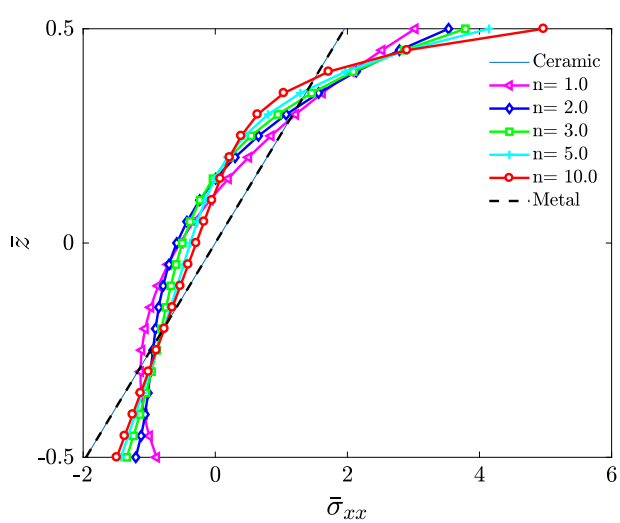

Fig. 12 Through-thickness variation of in-plane axial $\bar{\sigma}_{xx}$ under UDL using RM ($a/h = 10$, SS1 BC)

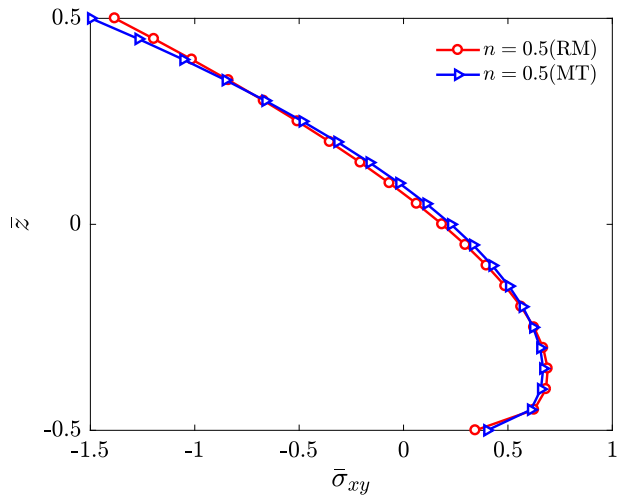

Fig. 13 Comparison of through-thickness variation of in-plane shear stress $\bar{\sigma}_{xy}$ under UDL using RM and MT ($a/h = 10$, SS1 BC)

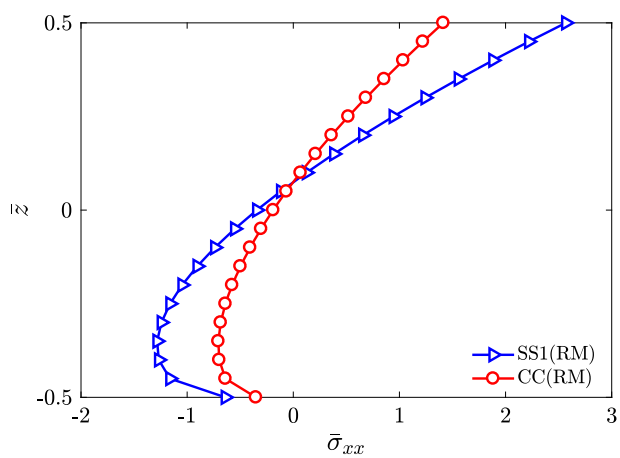

Fig. 14 Comparison of through-thickness variation of in-plane axial stress $\bar{\sigma}_{xz}$ under UDL using SS1 and CC boundary conditions ($a/h = 10$, $n = 0.5$)

5 Conclusions

The static bending analysis of FGM plates has been carried out using two different homogenization schemes, namely the Voigt model and the Mori–Tanaka scheme (to obtain the effective material properties through the thickness) to determine the influence of each homogenization scheme on the deflections and stresses. It is observed that the effective elastic properties estimated by the Voigt model are larger than those obtained with the Mori–Tanaka scheme. The difference varies with the change in power-law index n and is seen to be the highest for $n = 0.5$ to the tune of 11.5%. For the limiting cases the difference is negligible. The results obtained were compared with the analytical solution from [28], and it has been observed that the rule of mixtures give a better estimate of the elastic properties for values of $n = 0$–2.0, whereas Mori–Tanaka method predicts the elastic properties quite accurately for values above $n = 2.0$. The rule of mixture provides a conservative estimate, and this can be one of the reasons why most of the researchers have used rule of mixtures. The effect of boundary conditions (two simply supported cases: SS1 and SS2) on the deformations and stresses is very minimal. The clamped (CC) boundary conditions impart additional stiffness; hence, there is a drop in the deflections. The deflections increase with the increase in the power-law index n and decrease with the increase in the thickness of the plate.

References

1. Shen, H.-S.: Functionally Graded Materials: Nonlinear Analysis of Plates and Shells. CRC Press, Boca Raton (2009)
2. Jha, D.K., Kant, T., Singh, R.K.: A critical review of recent research on functionally graded plates. Compos. Struct. **96**, 833–849 (2013)
3. Birman, V., Byrd, L.W.: Modeling and analysis of functionally graded materials and structures. Appl. Mech. Rev. **60**(5), 195–216 (2007)
4. Gupta, A., Talha, M.: Recent developments in modeling and analysis of functionally graded materials and structures. Prog. Aerosp. Sci. **79**, 1–14 (2015)
5. Zuiker, J.R.: Functionally graded materials: choice of micromechanics model and limitations in property variation. Compos. Eng. **5**(7), 807–819 (1995)
6. Klusemann, B., Svendsen, B.: Homogenization methods for multi-phase elastic composites: comparison and benchmarks. Tech. Mech. **30**(4), 374–386 (2010)
7. Reiter, T., Dvorak, G.J.: Micro mechanical modeling of functionally graded materials. In: IUTAM Symposium on Transformation Problems in Composite and Active Materials. Solid Mechanics and Its Applications, vol. 60, pp. 173–184 (1998)
8. Gasik, M.M.: Micromechanical modelling of functionally graded materials. Comput. Mater. Sci. **13**(1–3), 42–55 (1998)
9. Reddy, J.N.: Analysis of functionally graded plates. Int. J. Numer. Meth. Eng. **47**(1–3), 663–684 (2000)
10. Praveen, G.N., Reddy, J.N.: Nonlinear transient thermoelastic analysis of functionally graded ceramic-metal plates. Int. J. Solids Struct. **35**(33), 4457–4476 (1998)
11. Hasin, Z.: Assessment of the self consistent scheme approximation: conductivity of particulate composites. J. Compos. Mater. **2**(3), 284–300 (1968)
12. Hasin, Z., Shtrikman, S.: A variational approach to the theory of elastic behavior of multiphase materials. J. Mech. Phys. Solids **11**(2), 127–140 (1963)
13. Vel, S.S., Batra, R.C.: Exact solution for thermoelastic deformations of functionally graded thick rectangular plates. AIAA J. **40**(7), 1421–1433 (2002)
14. Mori, T., Tanaka, K.: Average stress in matrix and average elastic energy of materials with misfitting inclusions. Acta Metall. **21**(5), 571–574 (1973)
15. Benveniste, Y.: A new approach to the application of Mori–Tanaka's theory in composite materials. Mech. Mater. **6**(2), 147–157 (1987)
16. Willis, J.R.: Bounds and self-consistent estimates for the overall properties of anisotropic composites. J. Mech. Phys. Solids **25**(3), 185–202 (1977)
17. Hill, R.: A self consistent mechanics of composite materials. J. Mech. Phys. Solids **13**(4), 213–222 (1965)
18. Bhaskar, K., Vardan, T.K.: The contradicting assumptions of zero transverse normal stress and strain in thin plate theory—a justification. J. Appl. Mech. **68**(4), 660–662 (2001)
19. Ferreira, A.J.M., Batra, R.C., Rouque, C.M.C., Qian, L.F., Martins, P.A.L.S.: Static analysis of functionally graded plates using third-order shear deformation theory and a meshless method. Compos. Struct. **69**(4), 449–457 (2005)
20. Shen, H.-S., Wang, Z.-X.: Assessment of Voigt and Mori–Tanaka models for vibration analysis of functionally graded plates. Compos. Struct. **94**(7), 2197–2208 (2012)
21. Ardestani, M.M., Soltani, B., Shams, Sh.: Analysis of functionally graded stiffened plates based on FSDT utilizing reproducing kernel particle method. Compos. Struct. **112**, 231–240 (2014)
22. Taj, G., Chakrabarti, A.: Static and dynamic analysis of functionally graded skew plates. J. Eng. Mech. **139**(7), 848–857 (2013)
23. Reddy, J.N., Chin, C.D.: Thermo mechanical analysis of functionally graded cylinders and plates. J. Therm. Stress. **21**(6), 593–626 (1998)
24. Reddy, J.N., Cheng, Z.-Q.: Three-dimensional thermomechanical deformations of functionally graded rectangular plates. Eur. J. Mech. A. Solids **20**(5), 841–855 (2001)
25. Kashtalyan, M.: Three-dimensional elasticity solution for bending of functionally graded rectangular plates. Eur. J. Mech. A. Solids **23**(5), 853–864 (2004)
26. Elishakoff, I., Gentilini, C.: Three-dimensional flexure of rectangular plates made of functionally graded materials. J. Appl. Mech. **72**(5), 788–791 (2005)
27. Reddy, J.N.: Energy Principles and Variational Methods in Applied Mechanics, 3rd edn. Wiley, New York (2017)
28. Zenkour, A.M.: Generalized shear deformation theory for bending analysis of functionally graded plates. Appl. Math. Model. **30**(1), 67–84 (2006)
29. Matsunaga, H.: Stress analysis of functionally graded plates subjected to thermal and mechanical loadings. Compos. Struct. **87**(4), 344–357 (2009)
30. Hosseini-Hashemi, S., Taher, H.R.D., Akhavan, H., Omidi, M.: Free vibration of functionally graded rectangular plates using first-order shear deformation plate theory. Appl. Math. Model. **34**(5), 1276–1291 (2010)
31. Talha, M., Singh, B.N.: Static response and free vibration analysis of FGM plates using higher order shear deformation theory. Appl. Math. Model. **34**(12), 3991–4011 (2010)
32. Singha, M.K., Prakash, T., Ganapathi, M.: Finite Element analysis of functionally graded plates under transverse load. Finite Elem. Anal. Des. **47**(4), 453–460 (2011)
33. Reddy, J.N.: Mechanics of Laminated Composite Plates and Shells: Theory and Analysis, 2nd edn. CRC Press, Boca Raton (2004)
34. Reddy, J.N.: Theory and Analysis of Elastic Plates and Shells, 2nd edn. CRC Press, Boca Raton (2007)
35. Cowper, G.R.: The shear coefficient in Timoshenko's beam theory. J. Appl. Mech. **33**(2), 335–340 (1966)
36. Neves, A.M.A., Ferreira, A.J.M., Carrera, E., Cinefra, M., Roque, C.M.C., Jorge, R.M.N., Soares, C.M.M.: Static, free vibration and buckling analysis of functionally graded plates using a quasi-3D higher-order shear deformation theory and a meshless technique. Compos. B Eng. **44**(1), 657–674 (2013)

37. Carrera, E., Brischetto, S., Cinefra, M., Soave, M.: Effects of thickness stretching in functionally graded plates and shells. Compos. B Eng. **42**(2), 123–133 (2011)

Publisher's Note Springer Nature remains neutral with regard to jurisdictional claims in published maps and institutional affiliations.